Matter, Volume *7*

Supplemental information

Genome-edited trees for high-performance engineered wood

Yu Liu, Gen Li, Yimin Mao, Yue Gao, Minhua Zhao, Alexandra Brozena, Derrick Wang, Samuel von Keitz, Taotao Meng, Hoon Kim, Xuejun Pan, Yiping Qi, and Liangbing Hu

Supplemental Figures

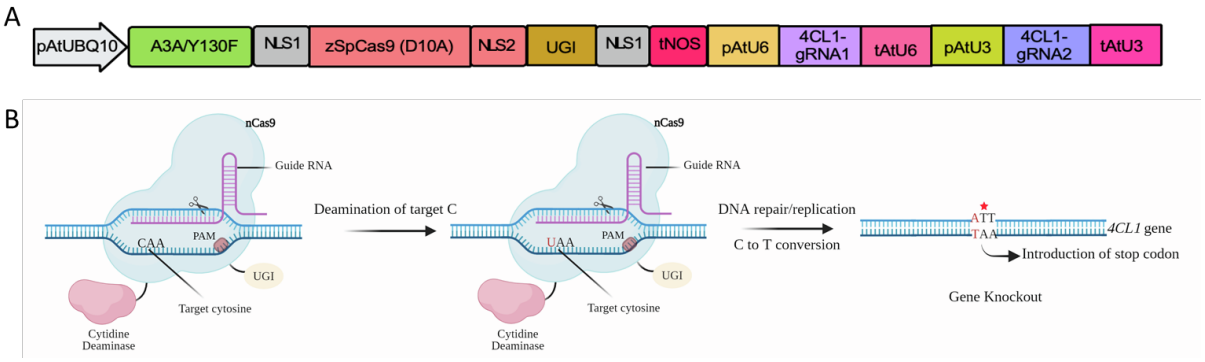

Figure S1. Gene knockout via C-to-T base editing system introducing premature stop codon. (A) Construct diagram of the nCas9-A3A/Y130F based CBE system targeting the poplar 4*CL1* gene using two gRNAs. (B) Illustration of the introduction of a premature stop codon via C-to-T base editing system. C-to-T base editor converts cytosine to uracil at the target site, which is further converted to thymine during DNA repair and replication. The C-to-T conversion introduces a premature stop codon TAA at the target site.

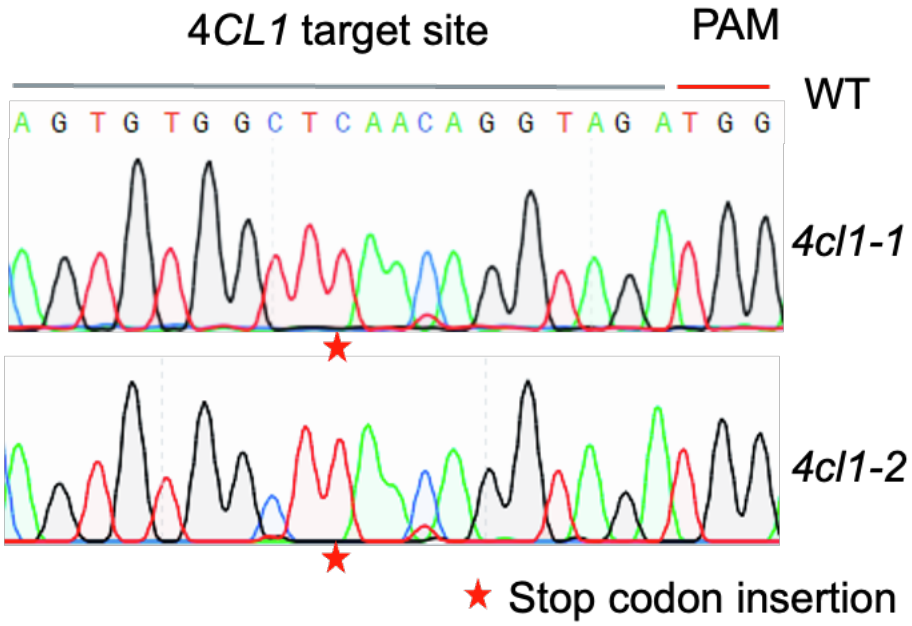

Figure S2. Genotype of the two 4*CL1* mutants. The red stars indicate the C-to-T mutation sites introducing the premature stop codon.

Figure S3. Phenotype of fresh wood from the 4*CL1* mutants and the natural tree, demonstrating the color change after *4CL1* knockout.

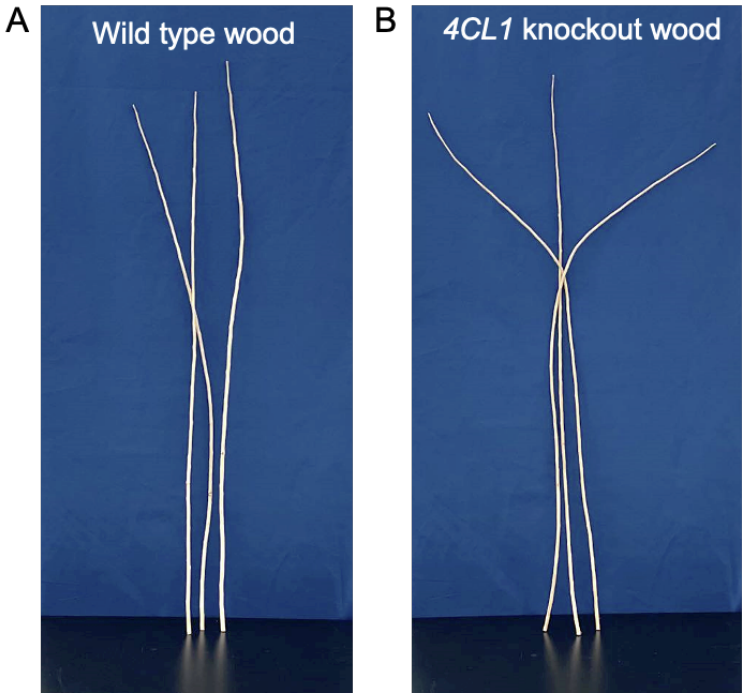

Figure S4. The images show the wood samples are of almost the same size and appearance. Photographs of dry (A) wild type wood and (B) *4CL1* Knockout wood obtained from 6-month growth trees, respectively, after bark removal.

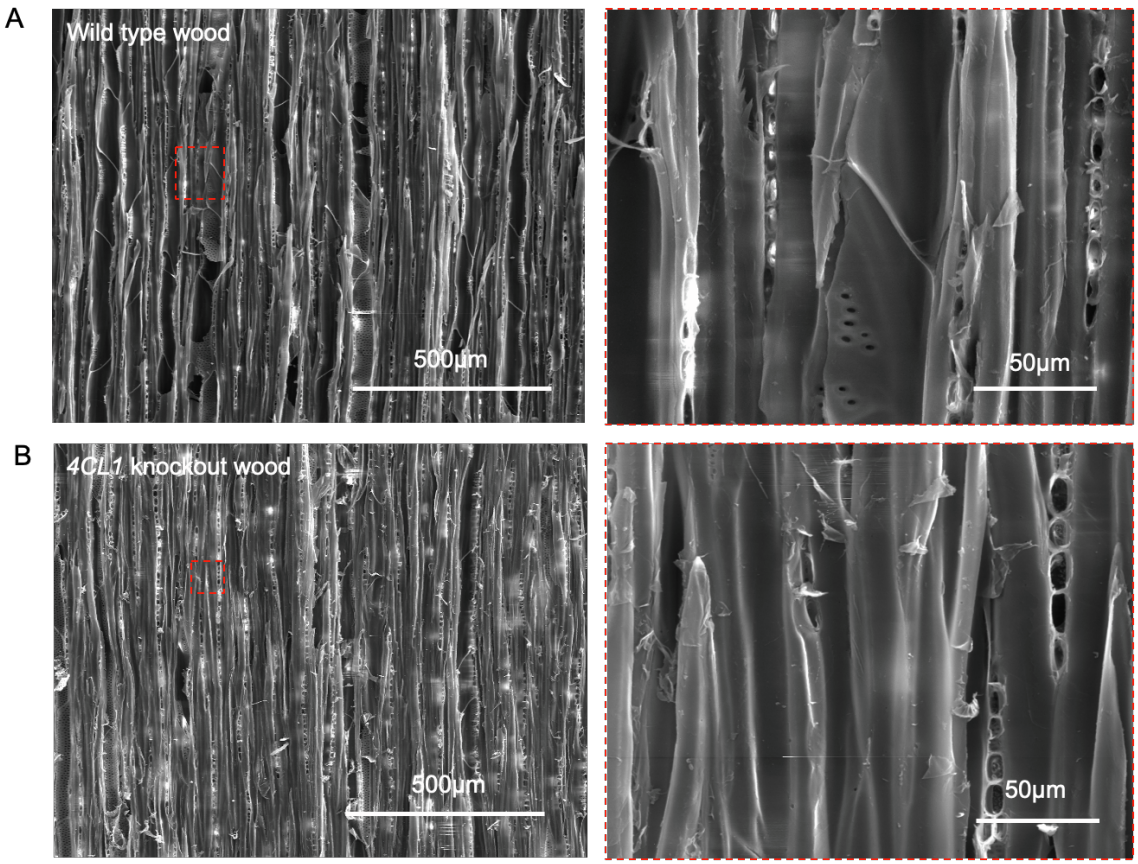

Figure S5. SEM images showing the cellulose fibers alignment of (A) wild type wood and (B) *4CL1* Knockout wood from the 6-month growth of wild type tree and *4CL1* Knockout tree to show the little change in structure of the wood samples after *4CL1* Knockout.

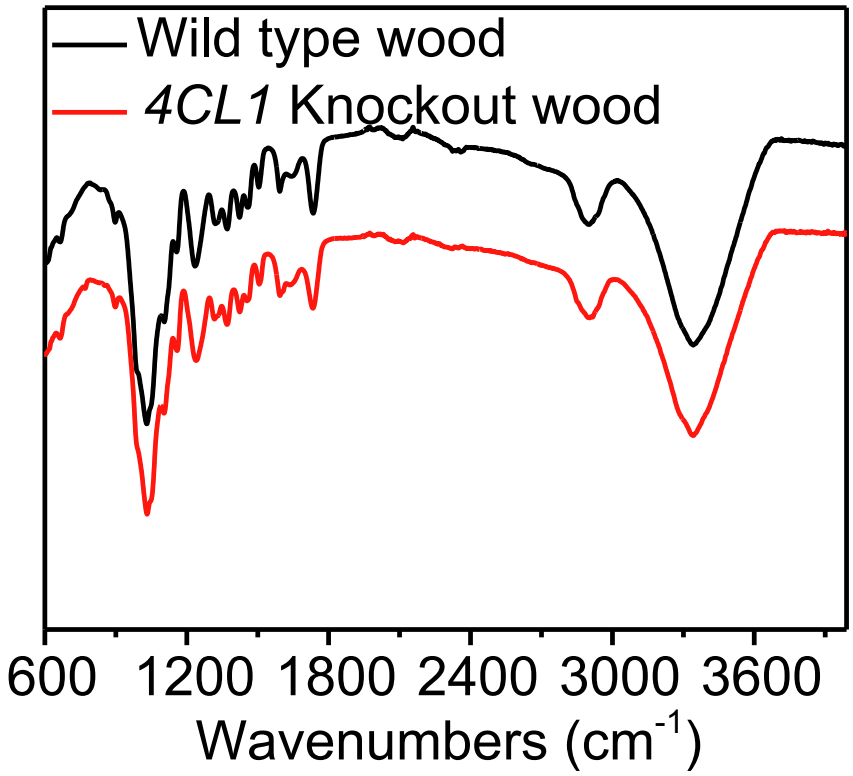

Figure S6. FTIR spectra of the wild type wood and *4CL1* Knockout wood demonstrating the main chemical component of wood samples before and after *4CL1* Knockout.

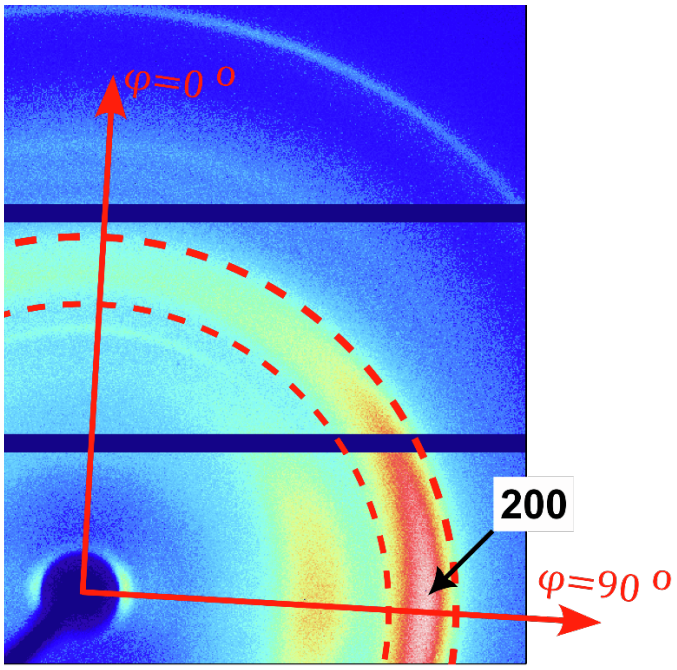

Figure S7. 2D WAXS image to show ϕ ranging from ϕ = 0° to ϕ = 90°. ϕ = 0° is aligned with the wood vertical growth direction.

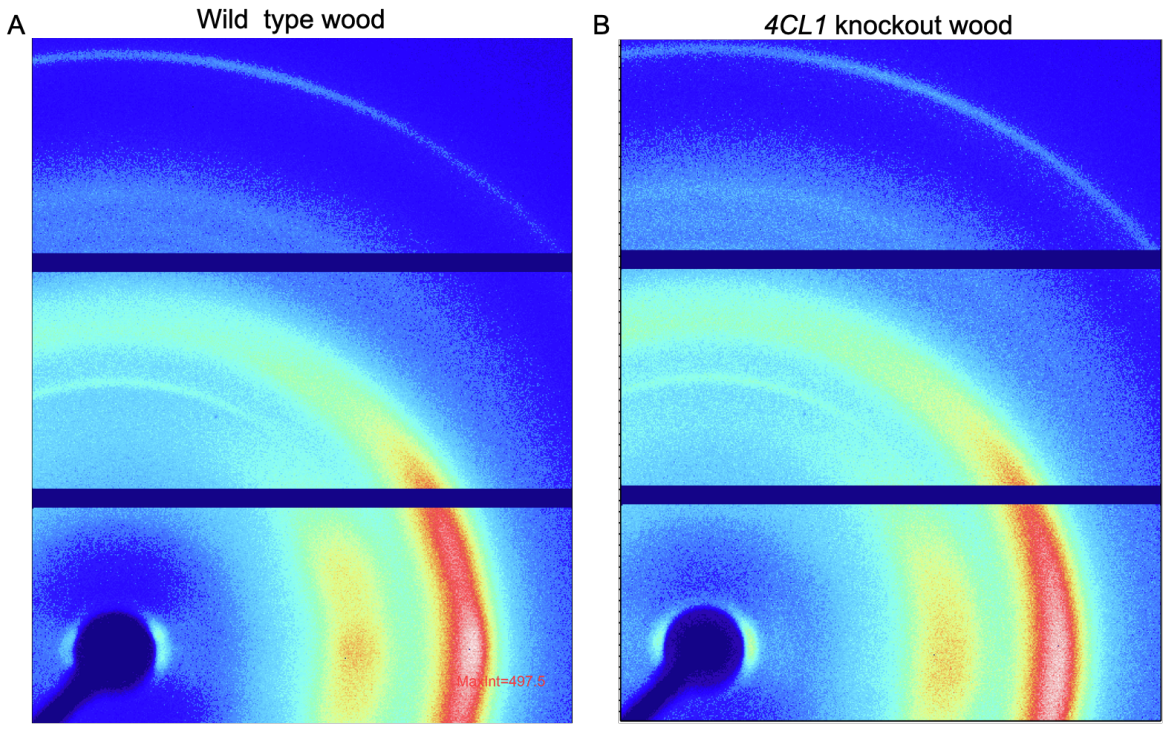

Figure S8. WXRD image of (A) wild type wood, (B) *4CL1* Knockout wood to compare the change in nano structure after *4CL1* Knockout.

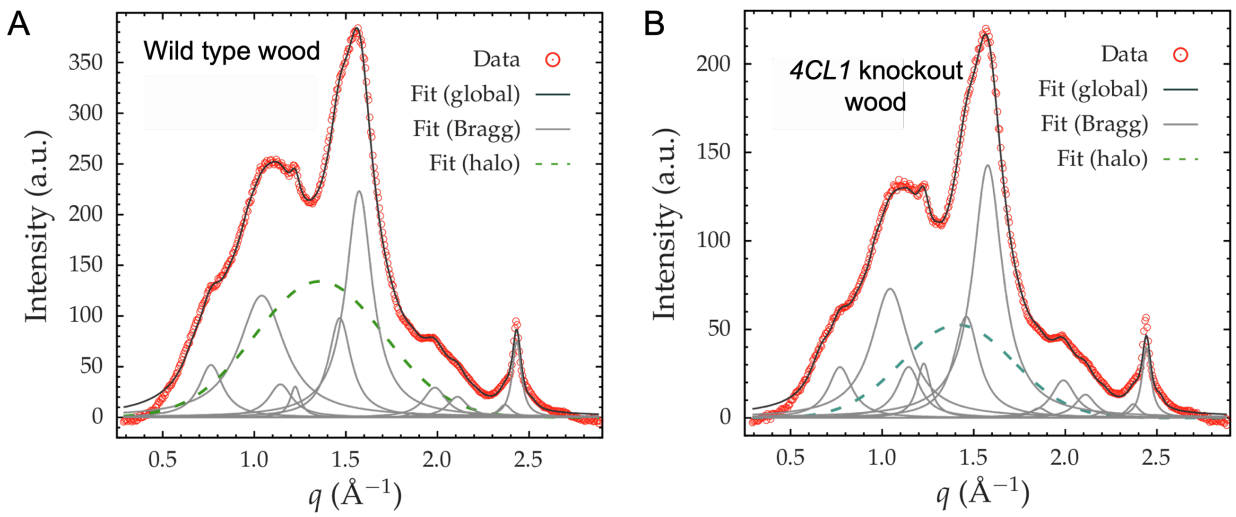

Figure S9. Determination of relative crystallinity index (RCI) of (A) wild type wood and (B) *4CL1* Knockout wood using WAXS.

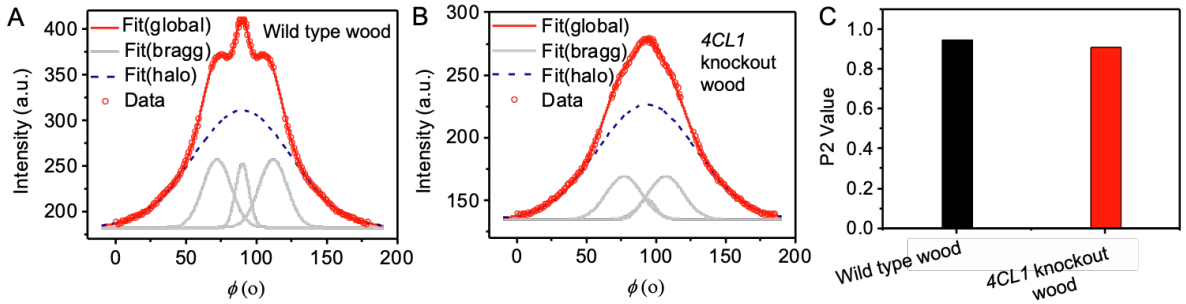

Figure S10. Determination of the P_2 value of wild type wood and *4CL1* knockout wood. (A), (B) Polar angle dependence of the WAXS scattering intensity within the q-range covering the 200 Bragg's peak; the intensity distributions are deconvoluted into two portions, attributed to the amorphous portion and crystalline portion, respectively. (C**)** Comparison of the P_2 value of wild type wood and *4CL1* Knockout wood.

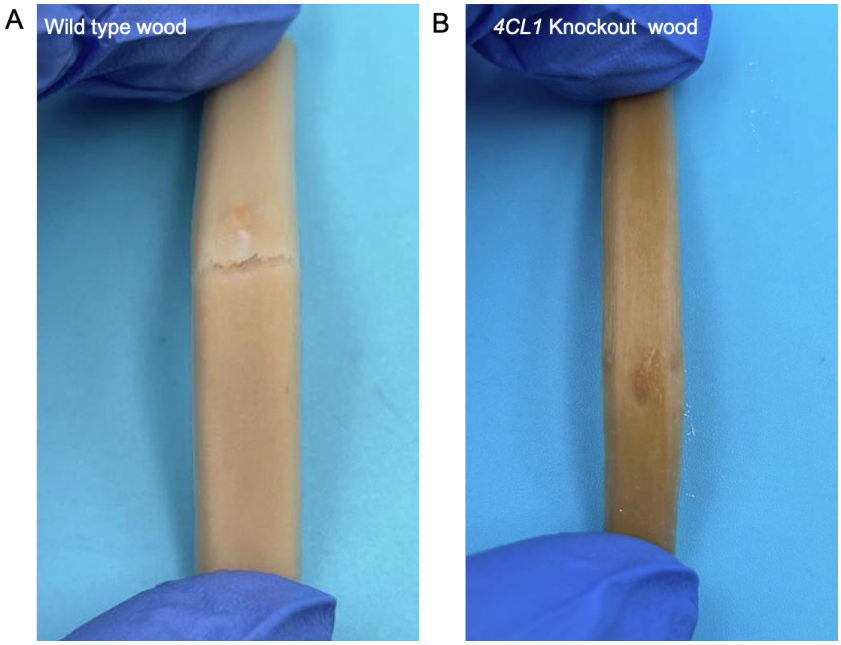

Figure S11. Comparison of the outlook of the two wood samples after bending by hand. Photo of the (A) wild type wood and (B) *4CL1* Knockout wood after bending by hand. The wild type wood easily cracks, while the *4CL1* Knockout wood remains in good condition without visible cracks.

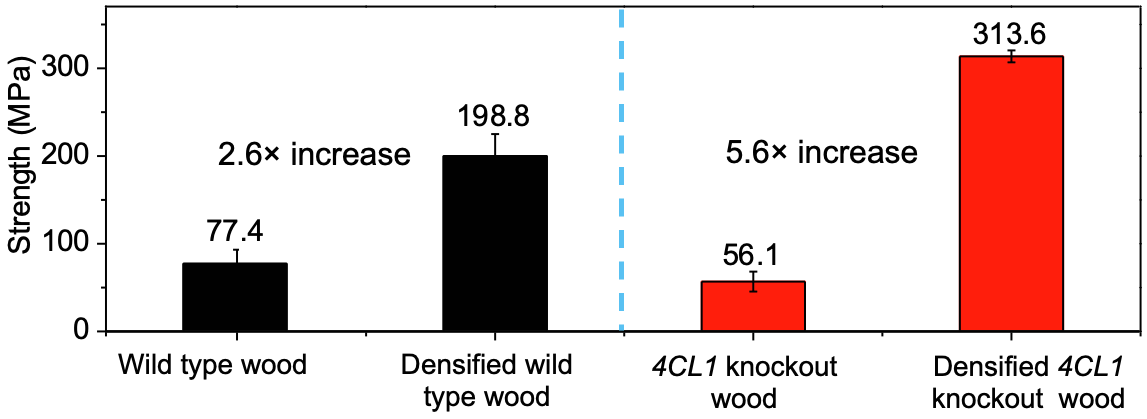

Figure S12. Comparison of the tensile strength of the wild type wood and *4CL1* Knockout wood, and densified wild type wood and densified *4CL1* Knockout wood.

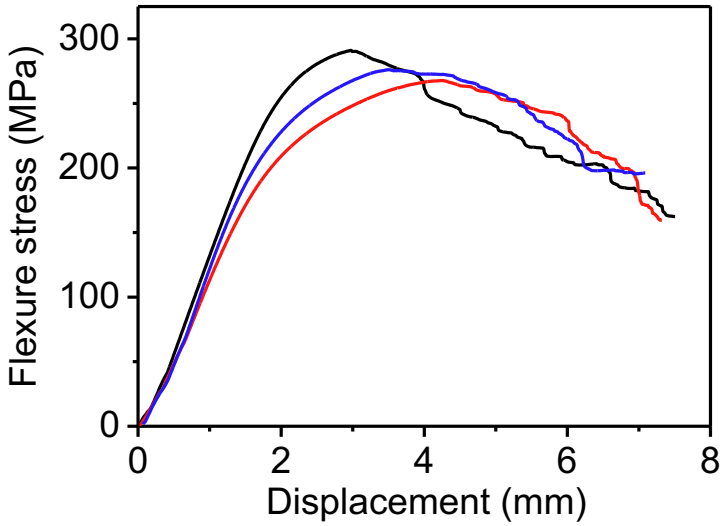

Figure S13. The three-point bending stress–displacement curves of the densified *4CL1* Knockout wood.

Supplemental Tables

Table S1 sgRNA target sequence of *4CL1* gene.

Name	sgRNA target sequence with PAM
4CL1-sgRNA1	TCCTCAGGCTAGACTTGGTC**AGG**
4CL2-sgRNA2	AGTGTGGCTCAACAGGTAGA**TGG**

Table S2 DNA Oligonucleotides used in this study.

Name	DNA oligonucleotides
4CL1-sgRNA1-F	5’-GGTCATCCTCAGGCTAGACTTGGTC-3’
4CL1-sgRNA1-R	5’-AAACGACCAAGTCTAGCCTGAGGAT-3’
4CL2-sgRNA2-F	5’-GGTCAGTGTGGCTCAACAGGTAGA-3’
4CL1-sgRNA2-R	5’-AAACTCTACCTGTTGAGCCACACT-3’
4CL1-Seq 1, 2-F	GCATTGCCTTATTCATCAGG
4CL1-Seq 1, 2-R	CAGTTGATCAAACAAGAATGGG

Supplemental Experimental Procedures

Orientation analysis using WAXS

Orientation of wood structures were analyzed via 2D WAXS method. The coordinate system is defined as in Fig. S7. ϕ denotes the polar angle, ranging from $\phi = 0°$ to $\phi = 90°$. $\phi = 0°$ is aligned with the wood vertical growth direction. The degree of fibril structure orientation can be quantified using Hermans orientation factor, P_2,

$$P_2 = \frac{1}{2}(3\langle \cos^2\phi\rangle - 1) \qquad \text{Eq S1}$$

In 2D WAXS, the 200 Bragg's peak was selected to compute P_2. The scattered intensity banking the 200 peak, as indicated in the dashed lines, was used to analyzing its polar angular dependence. Data fitting was based on the 1D profiles, showing the change of the scattered intensity, $\mathrm{I}_{200}(\phi)$, as a function of polar angle ϕ; and the $\langle \cos^2\phi\rangle$ term was calculated using Eq. S2.

$$\cos^2\phi\rangle = \frac{\int_0^{\pi/2} \mathrm{I}_{200}(\phi)\cdot\cos^2\phi\cdot\sin\phi \mathrm{d}\phi}{\int_0^{\pi/2} \mathrm{I}_{200}(\phi)\cdot\sin\phi \mathrm{d}\phi} \qquad \text{Eq S2}$$

Note that in Fig. S8 (A, B) besides the maximum scattered intensity located at $\phi = 90°$, two 'shoulders' appear at oblique angles with respect to center ($\phi = 90°$), which are attributed to cellulose fibril twisting angles, owing to the growth of elementary fibrils surrounding the cell wall in a spiral manner. These oblique angles are 17.9° and 16.4° for wild type wood and *4CL1* Knockout-wood, respectively. The values of the oblique angles are consistent with general observations in hardwood, as reported in various microscopic data. To count for the effect of twisting angle, the intensity distribution was deconvoluted into three components: a central broad peak due to amorphous materials, two shoulders at an oblique angle with respect to the center, in addition to the central peak at a lower intensity level, due to the 200 Bragg peak. The scattered intensity distribution of the three components are modeled using Gaussian probability functions; and the breath of the probability functions is associated with the degree of orientation, quantified by the Hermans oriention factor, P_2. The polar angle at the scattered intensity maxium was set as the reference axis; and P_2 varys between 0 and 1, with 0 refering to a status of random orientation, and 1 to the condition of perfect fibril alignment. Averages of the P_2 values due to the 200 Bragg peak, as obtained from the peak at the center and that at the obilique angles, were used to compare the degree of orientation of cellulose fibrils in wild type wood and that in *4CL1* Knockout wood. P_2 values for wild type wood was 0.95, and that of *4CL1* Knockout wood was 0.91.

Relative crystallinity index (RCI) determined using WAXS

RCI was determined from the 1D averaged scattering profile, namely, the scattered intensity versus q (scattering angle) profile, as shown in Fig. S6. The overall scattering traces can be deconvoluted into a series of Bragg peaks (light solid bell-shaped functions) and one broad amorphous halo (in green dashed line), and the RCI is defined as

$$\mathrm{RCI} = \frac{\Sigma \mathrm{A}_{\mathrm{Bragg}}}{\Sigma \mathrm{A}_{\mathrm{Bragg}} + \mathrm{A}_{halo}} \qquad \text{Eq S3}$$

$\mathrm{A}_{\mathrm{Bragg}}$s denotes the areas of the bell-shaped functions, which are modeled using Lorentzian probability distributions; and A_{halo} denote the area of the amorphous halo, modeled using a Gaussian function.

Note that due to intrinsic disorder in wild type wood and *4CL1* Knockout wood, the Bragg peaks are broad in general. Therefore, it is unnecessary to position the Bragg peaks based strictly on their theoretical scattering angles; rather, the ratio between the area of all Bragg peaks and the total area is of interest.